

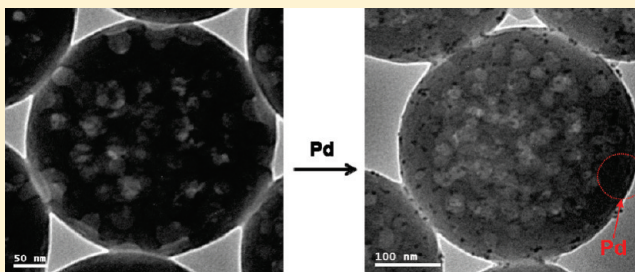
# One-Stage Synthesis of Cagelike Porous Polymeric Microspheres and Application as Catalyst Scaffold of Pd Nanoparticles

Jianxiong Xu, Guojun Chen, Rui Yan, Da Wang, Minchao Zhang, Wangqing Zhang,\* and Pingchuan Sun

Key Laboratory of Functional Polymer Materials of the Ministry of Education, Institute of Polymer Chemistry, Nankai University, Tianjin 300071, China

## Supporting Information

**ABSTRACT:** One-stage synthesis of cagelike porous polymeric microspheres and their application as catalyst scaffold of Pd nanoparticles are discussed. The synthesis of cagelike porous polymeric microspheres is achieved by W/O/W emulsion polymerization of a surfactant monomer of *N*-(4-vinylbenzyl)-*N*,*N*-dibutylamine hydrochloride and a hydrophobic monomer of styrene in water. Ascribed to the surfactant monomer, convenient one-stage synthesis of cagelike porous polymeric microspheres is afforded, and cagelike porous polymeric microspheres with size ranging from 300 to 600 nm and pore volume as large as 0.31 cm<sup>3</sup>/g are fabricated. The porous character and the inherent quaternary ammonium moieties make the cagelike porous polymeric microspheres to be the promising catalyst scaffold of Pd nanoparticles, and up to 10 wt % Pd catalyst with the metal particle size ranging from 2.1 to 5.7 nm is loaded. The catalytic hydrogenation of nitrobenzene by H<sub>2</sub> demonstrates that the heterogeneous Pd catalyst is efficient and reusable.



## 1. INTRODUCTION

The application of polymer as catalyst scaffold can be traced as early as the 1960s.<sup>1</sup> Since then, various polymeric materials including resins,<sup>2–5</sup> porous polymer,<sup>6–9</sup> nano- and microspheres,<sup>10–18</sup> dendrimer,<sup>19–21</sup> and even some soluble polymers<sup>22,23</sup> have been designed to support catalyst of noble metal nanoparticles. Compared with the inorganic support such as charcoal,<sup>24</sup> clay,<sup>25</sup> and metal oxides including silica and zeolites,<sup>26</sup> the polymeric scaffold has the advantages that the chemical composition, size, morphology, and even the penetrability or accessibility of the polymeric scaffold can be tailored.<sup>27–29</sup> Of all the polymeric catalyst scaffolds, the porous microspheres may be one of the most interesting candidates since the porous character provides good accessibility for reactants just as the micro- and mesoporous inorganic support.<sup>30–35</sup> Up to now, various porous polymeric microspheres including hollow microspheres have been fabricated and employed as scaffold for Pd, Au, Pt, Ag, and Rh nanocatalysts.<sup>30–36</sup> We have demonstrated that hollow polymeric microspheres act as not only the catalyst scaffold for noble metal nanoparticles but also the microcapsules for reactants; thus, the hollow polymeric microspheres containing the immobilized catalyst can be used as microreactor within which catalysis runs highly efficient.<sup>34–36</sup> However, the synthesis of porous polymeric microspheres generally involves multiple and complex procedures.<sup>34–46</sup> For examples, the general method to fabricate hollow microspheres by template polymerization includes synthesis of a suitable template particle, polymerization of the shell-forming monomer on the surface of the template particle to form coated microspheres, and removal of the

template by solvent etching.<sup>34–42</sup> Thus, convenient synthesis of porous polymeric microspheres is urgently needed in catalysis.

Interfacial polymerization through emulsion system such as oil-in-water-in-oil (O/W/O) emulsion and water-in-oil-in-water (W/O/W) emulsion has been proved to be an efficient method to produce porous microspheres, in which a binary surfactant mixture or a unitary surfactant is usually needed.<sup>47–54</sup> For example, the typical methods for making W/O/W emulsions use a two-step process of initial formation of an inverse water-in-oil emulsion and subsequent emulsification in water using a combination of two surfactants.<sup>49</sup> Improved methods using a unitary surfactant to construct W/O/W emulsion are also proposed, and various porous polymeric microspheres have been synthesized.<sup>51,52</sup> Different from the template polymerization employing a hard template to prepare hollow microspheres, a soft template such as surfactant micelles or oil drops is used in the W/O/W emulsion polymerization, and thus template elimination is avoided.<sup>47–54</sup> However, the removal of the surfactants and isolation of the resultant porous microspheres often involve repetitious centrifugation, washing, and redispersion, which limits their practical application.

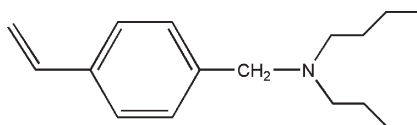
Herein, a convenient one-stage synthesis of cagelike porous polymeric microspheres containing the polystyrene (PS) and poly[*N*-(4-vinylbenzyl)-*N*,*N*-dibutylamine hydrochloride] (PVBAH) segments through W/O/W emulsion polymerization

**Received:** February 11, 2011

**Revised:** April 18, 2011

**Published:** April 22, 2011

Scheme 1. Chemical Structure of VBA



of a surfactant monomer of *N*-(4-vinylbenzyl)-*N,N*-dibutylamine hydrochloride (VBAH) and a hydrophobic monomer of styrene is reported. Ascribed to the VBAH surfactant monomer, the PS-*co*-PVBAH cagelike porous microspheres can be easily prepared without additional surfactant. Also ascribed to the VBAH surfactant monomer, the palladium precursor can be immobilized within the PS-*co*-PVBAH cagelike porous microspheres through ion exchange in the aqueous phase, and therefore the catalyst of Pd nanoparticles immobilized on cagelike porous microspheres is fabricated by the subsequent reduction with NaBH<sub>4</sub> aqueous solution. Catalyzed hydrogenation of nitrobenzene demonstrated that the resultant heterogeneous Pd catalyst is efficient and reusable.

## 2. EXPERIMENTAL SECTION

**2.1. Materials.** Styrene (St, >98%, Tianjin Chemical Co.) was distilled under vacuum before being used. The reagents including *n*-dibutylamine (DBA, >98%, Alfa), chloromethylstyrene (CMS, >97%, Alfa), polyvinylpyrrolidone (PVP, *M*<sub>w</sub> = 10 000, BASF), K<sub>2</sub>S<sub>2</sub>O<sub>8</sub> (>99.5%, Tianjin Chemical Co.), PdCl<sub>2</sub> (>99%, Alfa), NaBH<sub>4</sub> (>99%, Tianjin Chemical Co.), nitrobenzene (99%, Tianjin Chemical Co.), and phenylamine (99%, Tianjin Chemical Co.) were used as received. All the other chemical reagents were analytic grade and used as received.

**2.2. Synthesis of *N*-(4-Vinylbenzyl)-*N,N*-dibutylamine (VBA).** Into a flask CMS (30.4 g, 0.20 mol), DBA (51.6 g, 0.40 mol), K<sub>2</sub>CO<sub>3</sub> (48.8 g, 0.40 mol), and 200 mL of CHCl<sub>3</sub> were sequentially added. The flask content was initially degassed by nitrogen purge and then heated at 50 °C for 24 h with magnetic stirring. After completion of the reaction, the mixture was poured into 500 mL of water, and then the organic phase was collected. The collected organic phase was initially dried over anhydrous magnesium sulfate, and then the solvent is removed by rotary evaporation under vacuum at room temperature to obtain a crude product. Lastly, the crude product was purified by column chromatography using the solvent mixture of petroleum ether and ethyl acetate (6:1 by volume) to afford 30.1 g (69% yield) of a light-yellow liquid of VBA (Scheme 1). <sup>1</sup>H NMR (CDCl<sub>3</sub>): δ 7.41 (d, *J* = 8.3 Hz, 2H), 7.32 (d, *J* = 8.3 Hz, 2H), 6.72 (dd, 11.0, 17.8 Hz, 1H), 5.77 (dd, 17.8, 0.8 Hz, 1H), 5.27 (dd, 0.8, 11 Hz, 1H), 3.62 (s, 2H), 2.36 (t, *J* = 8 Hz, 4H), 1.42–1.31 (m, 8H), 0.96 (t, *J* = 7.4 Hz, 6H).

**2.3. Synthesis of the PS-*co*-PVBAH Cagelike Porous Microspheres.** Into a glass flask a given amount of VBA and a given volume of water ranging from 100 to 400 mL were initially added. Subsequently, HCl aqueous solution (10 mL, 0.1–1 mol/L) was added dropwise with magnetic stirring until a clear solution was observed at pH = 7. Then, St (5.2 g, 50 mmol) and PVP (0.3 g) were added with vigorous stirring for 30 min to form a stable emulsion. The flask content was initially degassed under nitrogen purge to remove oxygen, then heated at 80 °C, and followed by addition of K<sub>2</sub>S<sub>2</sub>O<sub>8</sub> (0.15 g, 0.55 mmol). The polymerization was performed under a nitrogen atmosphere with vigorous stirring for 20 h at 80 °C. After completion of the polymerization, the product was washed with ethanol (20 mL × 3), collected by centrifugation, and dried under vacuum at 40 °C to obtain the PS-*co*-PVBAH cagelike porous microspheres.

**2.4. Immobilization of Pd Nanoparticles on the PS-*co*-PVBAH Cagelike Porous Microspheres.** A given weight of PdCl<sub>2</sub> was initially dissolved in 15.0 mL of ethanol. Then, 0.133 g of the PS-*co*-PVBAH cagelike porous microspheres, which were synthesized at pH = 7 with the weight ratio of the feeding monomers to the solvent of water (O/W) = 2/100 and the weight ratio of VBA/St = 10/100 as discussed above, was added. The dispersion was kept at room temperature for 2 h with magnetic stirring, and then cool NaBH<sub>4</sub> aqueous solution (7.5 mL, 5–50 mmol/mL) was added, in which the molar ratio of NaBH<sub>4</sub>/PdCl<sub>2</sub> was set at 5:1. The resultant black dispersion was initially dialyzed against water for 3 days to remove the organic solvent of ethanol and the excessive NaBH<sub>4</sub>, and then the aqueous dispersion was diluted with water to a predetermined volume to obtain the aqueous dispersion of Pd nanoparticles immobilized on PS-*co*-PVBAH cagelike porous microspheres (Pd@PS-*co*-PVBAH).

By varying the weight ratio of PdCl<sub>2</sub> to the PS-*co*-PVBAH cagelike porous microspheres, four Pd@PS-*co*-PVBAH catalysts called 1-Pd@PS-*co*-PVBAH, 2-Pd@PS-*co*-PVBAH, 5-Pd@PS-*co*-PVBAH, and 10-Pd@PS-*co*-PVBAH with the weight ratio at 1.0%, 2.0%, 5.0%, and 10.0% were fabricated.

**2.5. Catalyst Testing.** The hydrogenation of nitrobenzene at 30 °C in aqueous dispersion by bubbling H<sub>2</sub> under a atmosphere pressure was employed to test the typical 10-Pd@PS-*co*-PVBAH catalyst. In the hydrogenation of nitrobenzene, 10 mL of aqueous dispersion of the 10-Pd@PS-*co*-PVBAH catalyst containing 5.0 × 10<sup>-3</sup> mmol of Pd was added into a 25 mL tubelike glass reactor equipped with a reflux condenser and a magnetic stirrer, and then the 10-Pd@PS-*co*-PVBAH catalyst was activated at 30 °C by bubbling H<sub>2</sub> (0.01 cm<sup>3</sup>/min) for 1 h. Hydrogenation by bubbling H<sub>2</sub> (0.01 cm<sup>3</sup>/min) was started immediately after addition of a given amount of nitrobenzene (0.06–0.30 g, 0.5–2.5 mmol). The molar ratio of C/S, in which C represents the Pd catalyst and S represents the substrate of nitrobenzene, ranges from 0.2% to 1.0%. To monitor the conversion of nitrobenzene and the yield of phenylamine, aliquots of the reaction mixture were withdrawn at given time intervals and analyzed by high-performance liquid chromatography (HPLC).

To detect Pd leaching from the typical 10-Pd@PS-*co*-PVBAH catalyst into the aqueous phase, the hydrogenation in aqueous dispersion at 30 °C with the molar ratio C/S = 0.5% was checked. After 20 min hydrogenation, the reaction mixture was filtered at the reaction temperature and the filtrate was collected. Part of the filtrate was further bubbled with H<sub>2</sub> (0.01 cm<sup>3</sup>/min) at 30 °C and the hydrogenation was monitored with HPLC, and part of the filtrate was analyzed by atomic absorption spectroscopy (AAS analysis).

To check the reuse of the typical 10-Pd@PS-*co*-PVBAH catalyst, after the hydrogenation of nitrobenzene at 30 °C with the molar ratio C/S = 0.5% was just completed in 90 min, the mixture was cooled to room temperature instantly. Subsequently, the product was extracted from the reaction mixture with cyclohexane (20 mL × 3), and then the organic phase was removed. The 10-Pd@PS-*co*-PVBAH catalyst remaining in the aqueous phase was reused in another run of hydrogenation of nitrobenzene under the same experiment conditions as in the fresh run. To diagnose possible aggregation of the Pd nanoparticles in the 10-Pd@PS-*co*-PVBAH catalyst, the aqueous dispersion of the recycled catalyst was detected by transmission electron microscopy (TEM).

**2.6. Characterization.** The scanning electron microscopy (SEM) images were obtained with a Shimadzu SS-550 microscope. Transmission electron microscopy (TEM) observation was performed using a Philips T20ST electron microscope at an acceleration of 200 kV, whereby a small drop of the aqueous dispersion of the synthesized microspheres was deposited onto a piece of copper grid and then dried at room temperature under vacuum. The nitrogen adsorption was performed on a Micromeritics Gemini V system at 77 K. The specific surface area was calculated by BET (Brunauer–Emmett–Teller)

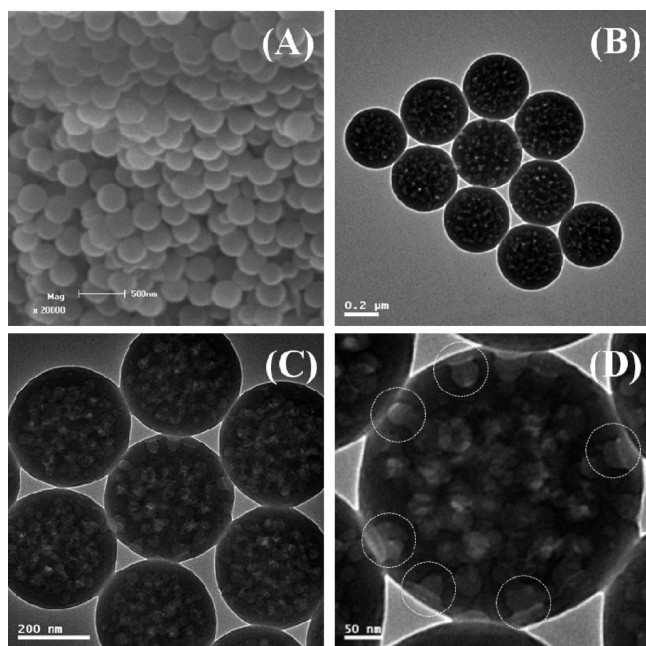


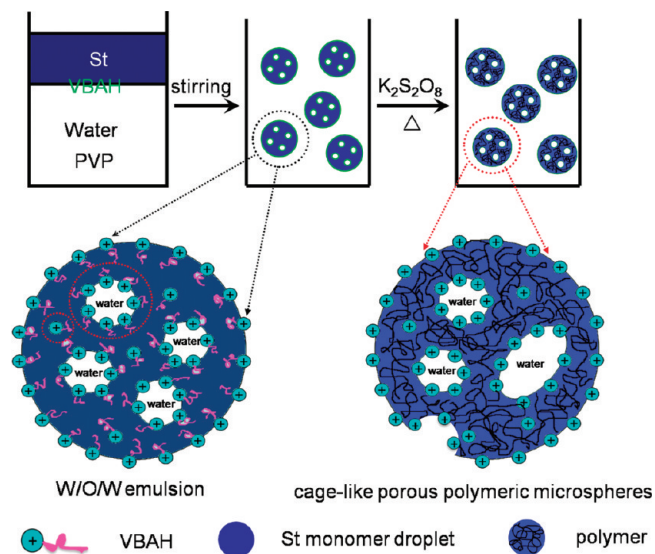
**Figure 1.** SEM (A) and TEM (B, C, D) images of the PS-*co*-PVBAH cage-like porous microspheres synthesized at pH = 7, VBA/St = 10/100, and O/W = 2/100.

method, the pore-size distribution was calculated from the adsorption branch using BJH (Barett–Joyner–Halenda) method, and total pore volume was obtained at  $p/p_0$  of 0.99. The  $^1\text{H}$  NMR spectrum was obtained on a 400 MHz spectrometer using  $\text{CDCl}_3$  as solvent. The solid state  $^{13}\text{C}$  CP/MAS NMR with TOSS was performed on a Varian Infinityplus-400 wide-bore (89 mm) NMR spectrometer equipped with a 4 mm double-resonance HX CP/MAS probe at a proton frequency of 400 MHz. The FTIR measurement was performed on a Bio-Rad FTS-6000 IR spectrometer. The powder X-ray diffraction (XRD) measurement was performed on a Rigaku D/max 2500 X-ray diffractometer. HPLC analysis was performed on a LabAlliance PC2001 system equipped with a C18 column and a UV–vis detector using a mixture of  $\text{CH}_3\text{CN}$  and water (6/4 by volume) as eluent. AAS analysis was performed on a Solaar AAS 2 atomic absorption spectrometer. The X-ray photoelectron spectroscopy (XPS) analyses were performed with a Kratos Axis Ultra DLD spectrometer employing a monochromated Al K $\alpha$  X-ray source (1486.6 eV) and a delay line detector (DLD).

### 3. RESULTS AND DISCUSSION

**3.1. Synthesis of the PS-*co*-PVBAH Cage-like Porous Microspheres.** The synthesis of the PS-*co*-PVBAH cage-like porous microspheres includes the construction of the W/O/W emulsion and the polymerization of the W/O/W emulsion initiated by the hydrophilic  $\text{K}_2\text{S}_2\text{O}_8$  to form colloids stabilized by PVP, which is schematically shown in Scheme 2. After mixing the surfactant monomer of VBAH and the hydrophobic monomer of St in water and followed vigorous stirring, the emulsifying W/O/W droplets, which are composed of the hydrophobic monomer of St and several encapsulated surfactant monomer micelles of VBAH (indicated by the large red cycle) as shown in Scheme 2, are formed. Furthermore, it is expected that some of the surfactant monomers locate on the surface of the emulsifying W/O/W droplets together with PVP to act as stabilizer, and a few of the surfactant monomers (indicated by the small red cycle in Scheme 2) are soluble in the emulsifying W/O/W droplets.

**Scheme 2.** Schematic One-Stage Synthesis of the PS-*co*-PVBAH Cage-like Porous Microspheres through the W/O/W Emulsion Polymerization

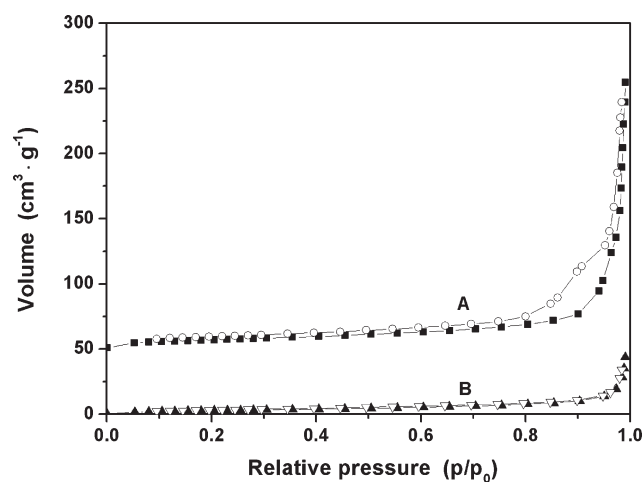


After the polymerization initiated by  $\text{K}_2\text{S}_2\text{O}_8$ , these emulsifying W/O/W droplets are converted into the PS-*co*-PVBAH cage-like porous microspheres which includes several macropores within the body as shown in Scheme 2.

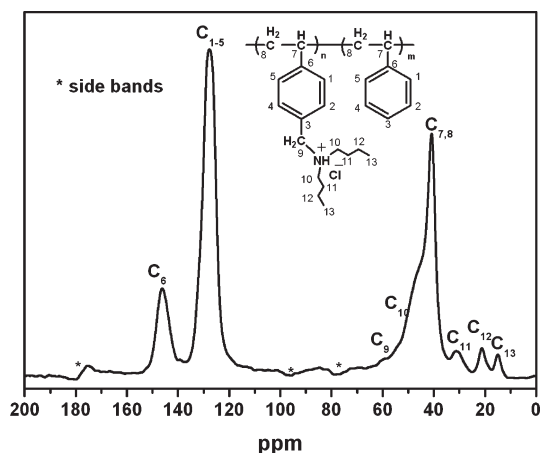
The parameters including the pH value of the aqueous phase, the monomer percent, or the weight ratio of the feeding monomers (St and VBA) to the solvent of water (O/W) and the weight ratio of VBA/St will affect the formation and the structure of the emulsifying W/O/W droplets and therefore further affect the synthesis of the PS-*co*-PVBAH cage-like porous microspheres. Thus, in the next discussion, synthesis of the PS-*co*-PVBAH cage-like porous microspheres under the optimized conditions is initially introduced, and subsequently the effect by the pH, the O/W value, and the VBA/St value on synthesis of the PS-*co*-PVBAH cage-like porous microspheres is discussed.

Figure 1 shows the SEM (A) and the TEM (B–D) images of the PS-*co*-PVBAH cage-like porous microspheres synthesized under the optimized conditions at pH = 7, O/W = 2/100, and VBA/St = 10/100. The SEM image (Figure 1A) shows that the synthesized PS-*co*-PVBAH cage-like porous microspheres have a uniform size distribution, and the average diameter is 350 nm. From the TEM images (Figures 1B–D), it is concluded that the PS-*co*-PVBAH cage-like porous microspheres containing lots of 20–50 nm macropores. The number of the macropores included in single PS-*co*-PVBAH cage-like porous microspheres ranges from 60 to 80. It is believed that the number of the macropores approximately corresponds to the amount of the surfactant monomer micelles in the W/O/W droplet. Besides, it is observed that some of the macropores are just located on the periphery of the cage-like porous microspheres (as indicated by the cycles in Figure 1D). These peripheral macropores together with the inner macropores make the cage-like porous microspheres accessible for reactants when they are used as catalyst scaffold.

Nitrogen adsorption is usually utilized to characterize porous materials.<sup>55</sup> To diagnose the porosity, the PS-*co*-PVBAH cage-like porous microspheres and the reference sample of the solid PS microspheres (Figure S1) which have the similar size and



**Figure 2.** Nitrogen adsorption–desorption isotherms of the PS-*co*-PVBAH cagelike porous microspheres (A) and the reference sample of the solid PS microspheres (B), in which the isotherm A was offset vertically by 50 cm<sup>3</sup>/g.



**Figure 3.** Solid-state <sup>13</sup>C CP/MAS NMR spectra of the PS-*co*-PVBAH cagelike porous microspheres.

chemical composition with the PS-*co*-PVBAH cagelike porous microspheres are characterized by nitrogen adsorption analysis. From the N<sub>2</sub> adsorption–desorption isotherms shown in Figure 2, an obvious hysteresis loop at 0.7–0.9  $p/p_0$  is observed for the PS-*co*-PVBAH cagelike porous microspheres (Figure 2A), whereas the reference sample of the solid PS microspheres exhibits a type I isotherm (Figure 2B). These results further confirm the porous character of the PS-*co*-PVBAH cagelike porous microspheres.<sup>55</sup> Ascribed to the porous character, the PS-*co*-PVBAH cagelike porous microspheres have a much larger pore volume (0.31 cm<sup>3</sup>/g vs 0.067 cm<sup>3</sup>/g) and a larger specific surface area (26.4 m<sup>2</sup>/g vs 10.6 m<sup>2</sup>/g) than those of the solid PS microspheres. The average pore size of the macropores calculated by the BJH method is about 46 nm, which is well-consistent with those measured by TEM observation shown in Figure 1. From the average size of the macropores measured by TEM and the pore volume calculated by BJH method, the number of the macropores including in single PS-*co*-PVBAH cagelike porous microspheres is evaluated to be ~100. The number is larger than that by TEM observation, since the TEM microscope

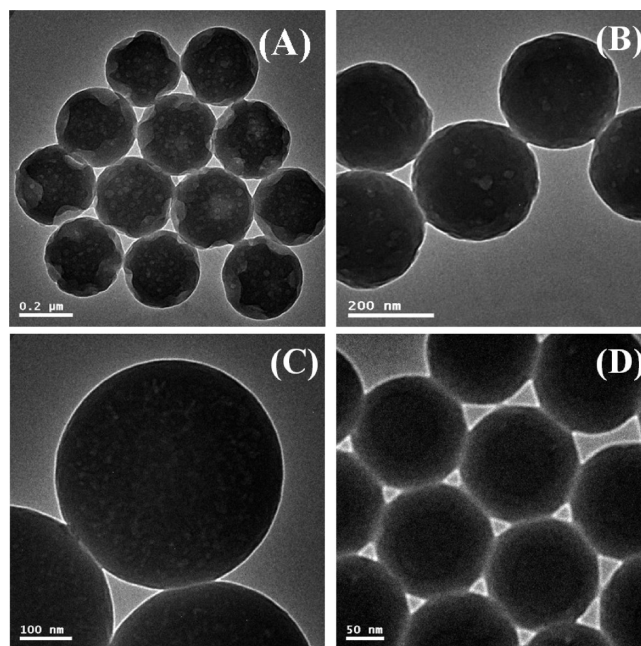


**Figure 4.** TEM images of the PS-*co*-PVBAH microspheres synthesized at pH = 1 (A), pH = 3 (B), pH = 7 (C), and pH > 7 (D) under the constant values of O/W = 3/100 and VBA/St = 10/100.

just shows an ichnographic image of the 3D cagelike porous microspheres.

To detect the chemical composition, the PS-*co*-PVBAH cagelike porous microspheres are characterized by solid <sup>13</sup>C CP/MAS NMR. As indicated by Figure 3, the characteristic chemical shifts due to the PS and the PVBAH segments are well recorded, confirming the chemical composition of the PS-*co*-PVBAH cagelike porous microspheres. In addition, the residual spinning side bands indicated as asterisks are also observed. The chemical composition of the PS-*co*-PVBAH cagelike porous microspheres is further confirmed by FTIR analysis (Figure S2).

**3.2. pH Effect on Synthesis of the Cagelike Porous Microspheres.** Because of the three long alkyl chains, the VBA monomer is insoluble in neutral water at room temperature. It is founded that when VBA is added into water, a thin yellow layer of the VBA monomer floating on water is optically observed even after vigorous stirring. Whereas, when HCl aqueous solution is added, VBA is acidified to form the surfactant monomer of VBAH, and the yellow layer floating on water gradually disappear until a pale opal dispersion is observed at pH = 7. Thus, the dispersion of VBA in water and therefore the construction of the W/O/W emulsion and the formation of the PS-*co*-PVBAH cagelike porous microspheres are pH-dependent. Figure 4 shows the TEM images of the PS-*co*-PVBAH colloids synthesized at different pH under the constant values of O/W = 3/100 and VBA/St = 10/100. Herein, it should be pointed out, when the VBA monomer is added into neutral water, the pH value of the aqueous phase is almost as same as those of the neutral water (pH = 7) since the VBA monomer cannot be dispersed in neutral water at all. To distinguish with the aqueous dispersion of the acidified monomer VBAH at pH = 7, the biphasic system of VBA and the neutral water is referred to pH > 7. As indicated in Figure 4A, core–shell porous microspheres are synthesized at pH = 1. The average size of the core–shell porous microspheres is 300 nm, and the average shell thickness is 40 nm. The

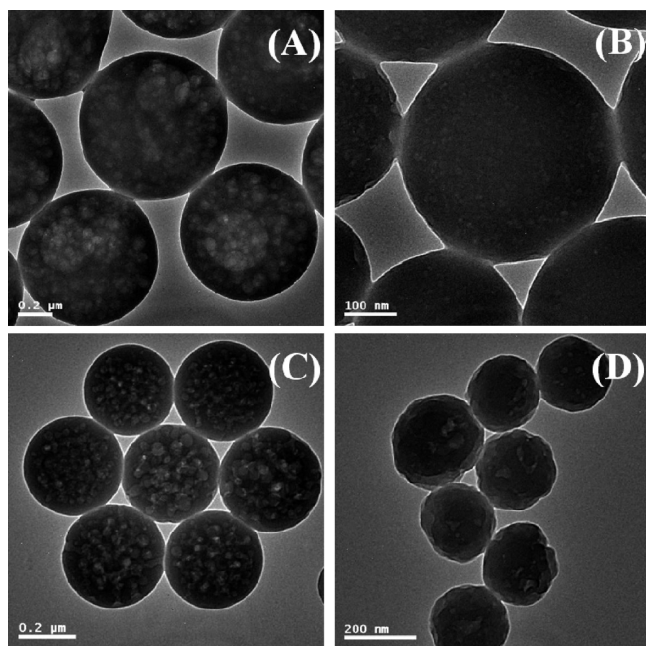


**Figure 5.** TEM images of the PS-*co*-PVBAH microspheres synthesized with weight ratio O/W of 6/100 (A), 3/100 (B), 2/100 (C), and 1.5/100 (D) at pH = 7 and VBA/St = 10/100.

core-shell porous microspheres are similar to the general core-shell microspheres synthesized by one-stage soap-free emulsion polymerization of the binary mixture of a hydrophobic monomer and a hydrophilic monomer in aqueous phase.<sup>56</sup> However, different from the general core-shell microspheres, macropores with size ranging from 10 to 30 nm are clearly observed in the present core-shell porous microspheres. The reason for the formation of core-shell porous microspheres at pH = 1 is discussed. At pH = 1, the VBA monomer is fully acidified, and it exists as both the unimer in aqueous phase and the surfactant micelles of VBAH encapsulated within the emulsifying W/O/W droplets. During the polymerization, the emulsifying W/O/W droplet converts into the porous core and the polymer resultant from the VBAH unimer deposits on the core to form the shell, and therefore core-shell porous microspheres as shown in Figure 4A are fabricated. When the pH value increases to 3, the balance between the unimer and the surfactant micelles of VBAH changes to the latter, and therefore 250 nm core-shell porous microspheres (Figure 4B) with a much more thin shell than those shown in Figure 4A (10 nm vs 40 nm) are produced. When the pH value further increases to 7, most of the VBAH surfactant monomer exists as surfactant micelles, and therefore the cagelike porous microspheres as shown in Figure 4C are synthesized. The present cagelike porous microspheres have almost the same morphology as those shown in Figure 1, except that the former has a slightly larger size (400 nm vs 350 nm). These results possibly suggest that high-concentrated monomer favors formation of large cagelike porous microspheres, which will be further discussed subsequently. When the VBA monomer is not acidified, it is insoluble in water but soluble in styrene, and therefore the W/O emulsion forms through vigorous stirring. After polymerization of the W/O emulsion, uniform solid microspheres, the average size of which is 150 nm as shown in Figure 4D, are fabricated. Interestingly, the TEM image (Figure 4D) shows that the solid PS-*co*-PVBA microspheres

have a core-shell structure, in which the core size is 80 nm and the shell thickness is 35 nm. We think the formation of the solid core-shell microspheres can be ascribed to the phase separation between the PS and the PVBA segments, since the PVBA and PS segments are incompatible due to their different hydrophilic/hydrophobic character. It is expected that the solid PS-*co*-PVBA core-shell microspheres have a PVBA-rich shell and PS-rich core, which are just as those core-shell microspheres synthesized by one-stage soap-free emulsion polymerization as discussed elsewhere.<sup>56</sup>

**3.3. Effect of the Oil/Water Weight Ratio on Synthesis of Cagelike Porous Microspheres.** Herein, the oil (O) represents the total feeding monomers of VBA and St. It is found that stable colloids can be synthesized when the O/W value is below 6/100 with pH = 7 and VBA/St = 10/100. Figure 5 shows the TEM images of the resultant PS-*co*-PVBAH microspheres synthesized with O/W ranging from 6/100 to 1.5/100 at pH = 7 and VBA/St = 10/100. The TEM observation confirms uniform cagelike porous microspheres can be fabricated within the O/W range from 6/100 to 2/100 (Figure 5A–C). When O/W decreases from 6/100 to 3/100 and further to 2/100, the average size of the resultant cagelike porous microspheres decreases from 600 nm (Figure 5A) to 400 nm (Figure 5B) and further to 350 nm (Figure 5C). Besides, it seems that the macropores in the cagelike porous microspheres synthesized at O/W = 6/100 are larger than those synthesized at O/W = 3/100 and O/W = 2/100. The formation of the large-sized macropores is possibly ascribed to the fusion of the single surfactant micelles during the W/O/W emulsion polymerization. Despite the different size of the macropores, the BJH analysis indicates that these three cagelike porous microspheres have the similar pore volume of 0.2–0.3 cm<sup>3</sup>/g. When O/W decreases to 1.5/100, core-shell porous microspheres (Figure 5D) similar to those shown in Figure 4B are fabricated. The formation of the core-shell porous microspheres under low O/W value of 1.5/100 at pH = 7 is similar to those under high O/W value of 3/100 at pH = 1–3, since the percent of the VBAH unimer in aqueous phase is high under the both synthesis cases.

**3.4. Effect of the VBA/St Weight Ratio on Synthesis of the Cagelike Porous Microspheres.** Clearly, the VBA/St weight ratio represents the percent of the surfactant monomer in the total monomers, and high VBA/St value represents high surfactant monomer percent in the resultant W/O/W emulsion. Polymerization under different VBA/St value at pH = 7 with a constant O/W = 3/100 value is checked. Figure 6 shows the TEM images of the resultant colloids synthesized with the VBA/St value ranging from 5/100 to 40/100. When VBA/St is 5/100, uniform solid PS-*co*-PVBAH microspheres (Figure 6A and Figure S3) without obvious porous structure are fabricated. The average size of the solid PS-*co*-PVBAH microspheres is 300 nm. The BJH analysis shows that the pore volume of the solid PS-*co*-PVBAH microspheres, 0.12 cm<sup>3</sup>/g, is little higher than those of the solid PS microspheres (Figure S1) but is lower than the PS-*co*-PVBAH cagelike porous microspheres synthesized at high VBA/St value shown in Figure 1. When the VBA/St value increases to 10/100 and further to 20/100, uniform cagelike porous microspheres with the average size of 400 nm (Figure 6B) and 500 nm (Figure 6C) are synthesized. The pore volume values of these two PS-*co*-PVBAH cagelike porous microspheres are estimated to be 0.22 and 0.30 cm<sup>3</sup>/g, which are larger than the solid PS-*co*-PVBAH microspheres (Figure 6A) as discussed above. Whereas, the latter PS-*co*-PVBAH cagelike

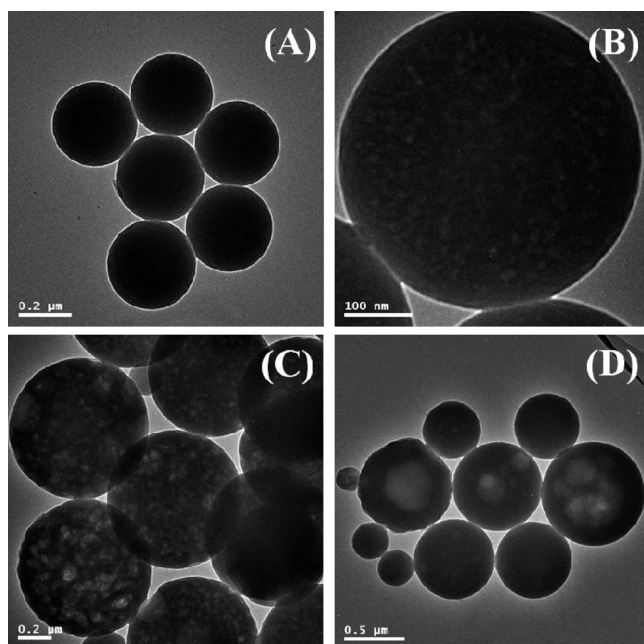


**Figure 6.** TEM images of the PS-*co*-PVBAH microspheres synthesized with weight ratio VBA/St of 5/100 (A), 10/100 (B), 20/100 (C) and 40/100 (D) at pH = 7 and O/W = 3/100.

porous microspheres synthesized at VBA/St = 20/100 have a larger average macropore size than the former ones synthesized at VBA/St = 10/100 (50 nm vs 15 nm), which is also confirmed by the TEM images shown in Figure 6B,C. These results suggest that when the VBA/St value increases from 5/100 to 20/100, colloids ranging from solid microspheres to cage-like porous microspheres are fabricated and the average size of the macropores increases with the increase in the VBA/St value. The possible reason is discussed. Under low VBA/St value of 5/100, most of the VBAH monomer exists as unimer in the emulsifying droplets, and therefore solid microspheres as shown in Figure 6A are fabricated. When the VBA/St value increases, the VBAH surfactant micelles instead of the unimers are encapsulated within the emulsifying W/O/W droplets, and therefore cage-like porous microspheres are fabricated. However, when the VBA/St value further increases to 40/100, the mixture of solid microspheres and cage-like porous microspheres including macropores as large as 200 nm (Figure 6D) are fabricated. Under a high VBA/St value of 40/100, only part of the VBAH surfactant monomer can be encapsulated within the emulsifying W/O/W droplets which will be converted into cage-like porous microspheres, and the residual VBAH surfactant monomer as well as some of the hydrophobic monomer of St forms the emulsifying W/O droplets which convert into solid microspheres after polymerization. Thus, the mixture of solid microspheres and cage-like porous microspheres as shown in Figure 6D are fabricated at high VBA/St value of 40/100.

**3.5. Immobilization of Pd Nanoparticles within the Cage-like Porous Microspheres.** Usually, immobilization of noble metal nanoparticles on the polymeric scaffold can be achieved initially by either coordination between the pendent ligands with the metal precursor or ion-exchange followed reduction with suitable reducing reactants.<sup>27–29</sup> Since the PS-*co*-PVBAH cage-like porous microspheres contain the PVBAH segment, it is expected that Pd catalyst can be immobilized through ion

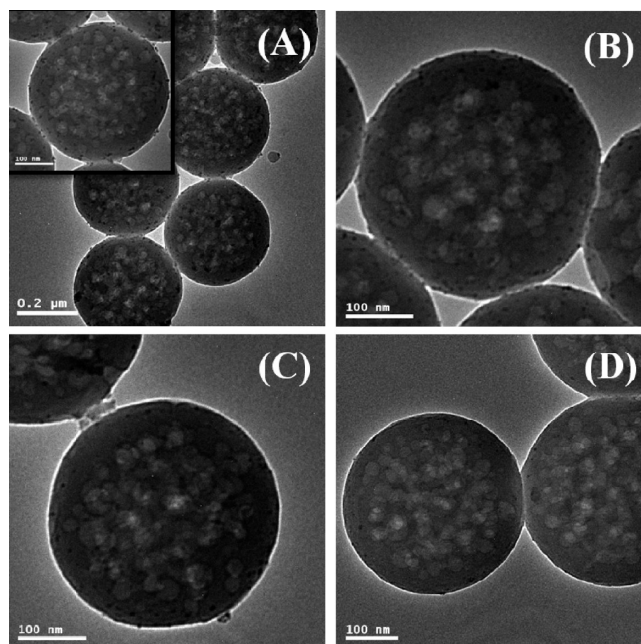


**Figure 7.** TEM images of the 10-Pd@PS-*co*-PVBAH (A), 5-Pd@PS-*co*-PVBAH (B), 2-Pd@PS-*co*-PVBAH (C), and 1-Pd@PS-*co*-PVBAH (D) catalysts.

exchange between the quaternary ammonium moieties in the PVBAH segment and the PdCl<sub>4</sub><sup>2-</sup> anions. Herein, the PS-*co*-PVBAH cage-like porous microspheres (Figure 1) synthesized at pH = 7, O/W = 2/100, and VBA/St = 10/100 are used as typical example to immobilize Pd nanoparticles. The present immobilization of Pd nanoparticles on the PS-*co*-PVBAH cage-like porous microspheres includes the ion exchange with the metal precursor and the subsequent reduction with NaBH<sub>4</sub> aqueous solution, which is very similar to those on the scaffold of the polymeric microspheres containing chelate ligands as discussed elsewhere.<sup>34–36,57</sup> By varying the weight ratio of PdCl<sub>2</sub> to the PS-*co*-PVBAH cage-like porous microspheres, four catalysts called 1-Pd@PS-*co*-PVBAH, 2-Pd@PS-*co*-PVBAH, 5-Pd@PS-*co*-PVBAH, and 10-Pd@PS-*co*-PVBAH are fabricated. Figure 7 shows the TEM images of the four Pd catalysts. As indicated, the resultant Pd nanoparticles are uniformly embedded in the PS-*co*-PVBAH cage-like porous microspheres in all the four cases, and almost no free Pd aggregates are observed even in the 10-Pd@PS-*co*-PVBAH catalyst (Figure 7A) with the weight ratio of PdCl<sub>2</sub> to the polymeric scaffold as high as 10%. However, when the weight ratio of PdCl<sub>2</sub> to the polymeric scaffold further increases to 15%, the loading of Pd catalyst is beyond the PS-*co*-PVBAH cage-like porous microspheres since black aggregates can be optically observed during the reduction. The average size of the immobilized Pd nanoparticles—2.1 nm for the 1-Pd@PS-*co*-PVBAH catalyst, 3.3 nm for the 2-Pd@PS-*co*-PVBAH catalyst, 5.1 nm for the 5-Pd@PS-*co*-PVBAH catalyst, and 5.7 nm for the 10-Pd@PS-*co*-PVBAH catalyst (Figures S4 and S5)—increases with the increase in the Pd content in the catalyst. The XPS analysis of the typical as-prepared 10-Pd@PS-*co*-PVBAH catalyst confirms that the catalytic metal exists as Pd nanoparticles (Figure S6).

The four catalysts including the 10-Pd@PS-*co*-PVBAH, 5-Pd@PS-*co*-PVBAH, 2-Pd@PS-*co*-PVBAH, and 1-Pd@PS-*co*-PVBAH are further characterized by XRD, and the XRD

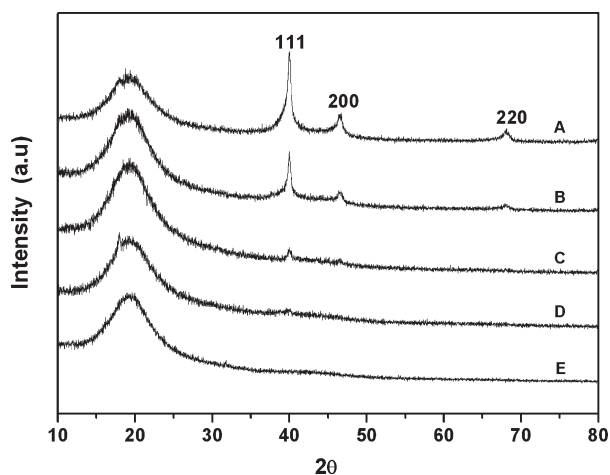


**Figure 8.** XRD patterns of the 10-Pd@PS-*co*-PVBAH (A), 5-Pd@PS-*co*-PVBAH (B), 2-Pd@PS-*co*-PVBAH (C), 1-Pd@PS-*co*-PVBAH catalyst (D), and the scaffold of the PS-*co*-PVBAH cage-like porous microspheres (E).

patterns are shown in Figure 8. For the 10-Pd@PS-*co*-PVBAH (Figure 8A) and 5-Pd@PS-*co*-PVBAH (Figure 8B) catalysts, three peaks at  $2\theta$  of  $40.0^\circ$ ,  $46.6^\circ$ , and  $68.0^\circ$  corresponding to the diffraction of the (111), (200), and (220) lattice planes of the Pd nanoparticles and the broad peak centered at  $2\theta$  of  $19.0^\circ$  corresponding to the amorphous polymeric scaffold of the PS-*co*-PVBAH cage-like porous microspheres can be clearly observed. According to the Scherrer equation,<sup>58</sup> the average size of the Pd nanoparticles is also evaluated utilizing the diffraction peak of (111) lattice plane, and the values, 7.6 nm for the 10-Pd@PS-*co*-PVBAH catalyst and 6.4 nm for the 5-Pd@PS-*co*-PVBAH catalyst, are slightly larger than those observed by TEM. For the 2-Pd@PS-*co*-PVBAH catalyst, possibly ascribed to the small size of the Pd nanoparticles and the low Pd content, the diffraction according to the immobilized Pd nanoparticles is very weak, and only a pale peak at  $2\theta$  of  $40.0^\circ$  is observed. When the size of the Pd nanoparticles and the Pd content further decrease, the 1-Pd@PS-*co*-PVBAH shows a XRD pattern (Figure 8D) similar to the polymeric scaffold itself (Figure 8E), from which no Pd diffraction but only the broad peak corresponding to the polymeric scaffold is observed.

**3.6. Catalyst Testing.** Hydrogenation of nitrobenzene to phenylamine is an industrially important transformation, since the product of phenylamine and its derivatives are widely used. The hydrogenation of nitrobenzene is generally achieved in organic solvent employing a heterogeneous Pd catalyst.<sup>59–65</sup> Various Pd catalysts including the Pd nanoparticles immobilized on inorganic support such as silica<sup>60,61</sup> and metal oxides<sup>59,62</sup> and polymeric support such as poly(3,6-dibenzaldimino-*N*-vinylcarbazole),<sup>63</sup> poly(vinylidene fluoride),<sup>64</sup> and polysiloxane<sup>65</sup> have been proposed for this transformation. It is deemed that the activity of the Pd catalyst is dependent on the support and the size of the Pd nanoparticles,<sup>59,62</sup> and generally small Pd nanoparticles present high catalytic activity.<sup>62</sup>

Herein, the typical catalyst of 10-Pd@PS-*co*-PVBAH, which is thought to be the most inefficient due to the largest size of the Pd nanoparticles in all the four catalysts, is used to evaluate the potential application of the PS-*co*-PVBAH cage-like porous microspheres as catalyst scaffold. Besides, since the 10-Pd@PS-*co*-PVBAH catalyst can be dispersed in water which is possibly ascribed to the porous structure (low density) and the PVBAH

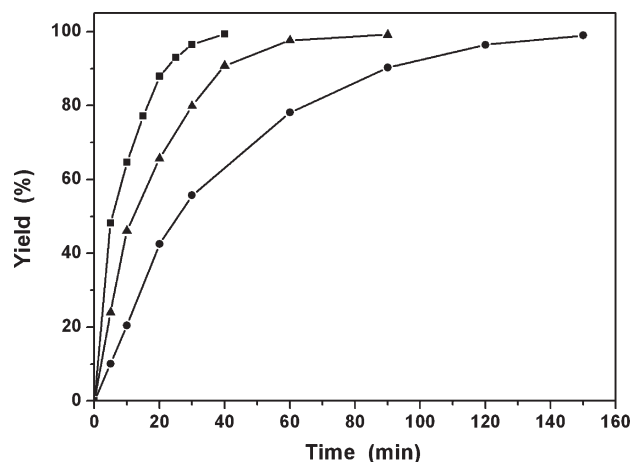


**Figure 9.** Time-dependent yield of phenylamine in the hydrogenation of nitrobenzene in water with the molar ratio C/S of 0.20% (●), 0.50% (▲), and 1.0% (■). Reaction conditions: nitrobenzene (0.06–0.30 g, 0.5–2.5 mmol), 10 mL of the aqueous dispersion of 10-Pd@PS-*co*-PVBAH containing  $5.0 \times 10^{-3}$  mmol of Pd catalyst,  $30^\circ\text{C}$ ,  $\text{H}_2$  (bubbling at atmospheric pressure,  $0.01\text{ cm}^3/\text{min}$ ).

segment, the hydrogenation is performed in water. Figure 9 shows the time-dependent yield of phenylamine in the hydrogenation of nitrobenzene with different molar ratio of C/S. It indicates that the hydrogenation of nitrobenzene can be completed in 40–150 min with the molar ratio C/S ranging from 1.0% to 0.20% and affords almost a quantitative yield of phenylamine. From Figure 9, the turnover frequency (TOF) value of the 10-Pd@PS-*co*-PVBAH catalyst,  $578\text{ h}^{-1}$  under the molar ratio C/S = 1.0%,  $576\text{ h}^{-1}$  under the molar ratio C/S = 0.50%, and  $606\text{ h}^{-1}$  under the molar ratio C/S = 0.20%, is calculated. Compared with the reference catalyst of Pd nanoparticles immobilized on the solid PS microspheres (Figure S7), the present 10-Pd@PS-*co*-PVBAH catalyst is much more efficient (TOF  $576\text{ h}^{-1}$  vs  $129\text{ h}^{-1}$ ). Compared with the hydrogenation of nitrobenzene catalyzed by the catalyst of Pd/gel nanocomposite under very similar conditions, the present hydrogenation runs much more fast (98% yield of phenylamine in 150 min vs >99% yield in 40 min),<sup>64</sup> confirming the highly efficient 10-Pd@PS-*co*-PVBAH catalyst.

The Pd catalyst leaching into aqueous phase has been further checked employing the hydrogenation of nitrobenzene in water at  $30^\circ\text{C}$  and with C/S = 0.5%. After the yield of phenylamine reaches 65.7% in 20 min, the 10-Pd@PS-*co*-PVBAH catalyst is initially isolated from the reaction mixture by filtration, then the liquid phase containing the reactant of nitrobenzene is bubbled with  $\text{H}_2$  at  $30^\circ\text{C}$  for a given time, and then the aqueous phase is analyzed by HPLC. As shown in Figure 10, when the 10-Pd@PS-*co*-PVBAH catalyst is removed from the reaction mixture, no further yield of phenylamine is observed in the next 70 min. Furthermore, no Pd in the aqueous phase is detected by AAS analysis (detection limit is 0.03 ppm). These results confirmed that the Pd catalyst leaching in the present reaction condition can be ignored. The much low Pd catalyst leaching into the aqueous solution is discussed, and it is ascribed to two reasons. First, most of the synthesized Pd nanoparticles are encapsulated within the matrix of the polymeric support of the PS-*co*-PVBAH cage-like porous microspheres as shown in Scheme 2, which decreases the catalyst leaching into aqueous solution. Second, in the present

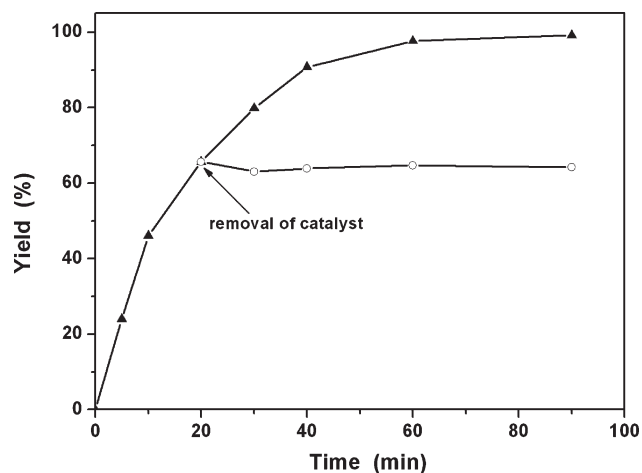


**Figure 10.** Time-dependent yield of phenylamine in the hydrogenation of nitrobenzene with the molar ratio  $C/S = 0.5\%$  (▲) and after the removal of the 10-Pd@PS-*co*-PVBAH catalyst (○). Reaction conditions can be found in the caption for Figure 9.

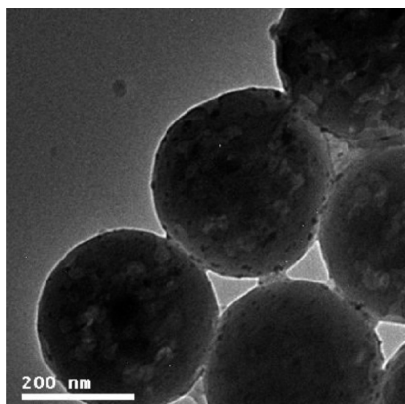


**Figure 11.** TEM image of the recycled 10-Pd@PS-*co*-PVBAH catalyst.

catalyzed hydrogenation, the balance between  $Pd^0$  and  $Pd^{2+}$  under bubbling  $H_2$  atmospheres favorably transfers to the former and therefore the catalyst leaching into aqueous is blocked.

Lastly, the recycling of the typical 10-Pd@PS-*co*-PVBAH catalyst is further studied. It is found that the 10-Pd@PS-*co*-PVBAH catalyst prefers being dispersed in the aqueous phase rather than in cyclohexane, while the substrate of nitrobenzene and the product of phenylamine are soluble in cyclohexane. The solubility difference of the Pd catalyst and the reactants makes an easy separation of the 10-Pd@PS-*co*-PVBAH catalyst by cyclohexane extraction and therefore affords convenient reuse of the Pd catalyst. After the hydrogenation of nitrobenzene at  $30\text{ }^\circ\text{C}$  with  $C/S = 0.5\%$  is just completed in 90 min (seeing the hydrogenation kinetics in Figure 9), the separated catalyst is reused in the next run. It is found that that the yield of phenylamine in 90 min keeps more or less the same ( $\sim 99\%$ ) even after four cycles of hydrogenation (Figure S8). The recycled catalyst is further characterized by TEM. As shown in Figure 11, the size and morphology of the PS-*co*-PVBAH cage-like porous microspheres in the recycled 10-Pd@PS-*co*-PVBAH catalyst remain as similar as those of the fresh ones, suggesting the stability of the polymeric scaffold. Furthermore, no clear Pd aggregation is observed in the recycled 10-Pd@PS-*co*-PVBAH catalyst, and the average size of the

Pd nanoparticles in the recycled catalyst is almost as the same as those in the fresh one, confirming the reusability of the 10-Pd@PS-*co*-PVBAH catalyst in the present conditions.

#### 4. CONCLUSIONS

A strategy of one-stage synthesis of cage-like porous microspheres containing macropores within the body through W/O/W emulsion polymerization of a surfactant monomer of VBAH and a hydrophobic monomer of St is proposed, and the application of the cage-like porous microspheres as catalyst scaffold of Pd nanoparticles is evaluated. The synthesis of cage-like porous microspheres includes the construction of the W/O/W emulsion in the presence of the VBAH surfactant monomer and the hydrophobic monomer of St in water and the subsequent polymerization initiated by the hydrophilic initiator of  $K_2S_2O_8$ . Ascribed to the VBAH surfactant monomer, formation of the W/O/W emulsion avoids additional ionic/nonionic surfactant and therefore affords a convenient one-stage synthesis of cage-like porous microspheres. The parameters affecting the synthesis of cage-like porous microspheres are explored. It is found that the pH value of the aqueous phase, the oil content, and the percent of the surfactant monomer in the W/O/W emulsion can greatly affect the synthesis of cage-like porous microspheres. By tuning the synthesis conditions, cage-like porous microspheres with size ranging from 300 to 600 nm and pore volume as large as  $0.31\text{ cm}^3/\text{g}$  are fabricated. The porous character and the inherent quaternary ammonium moieties in the cage-like porous microspheres make them to be the promising catalyst scaffold of Pd nanoparticles. Initially through ion exchange followed reduction with  $NaBH_4$  aqueous solution, 2.1–5.7 nm Pd nanoparticles are immobilized on the cage-like porous microspheres, and the loading of the Pd catalyst on the cage-like porous microspheres is up to 10 wt %. The catalytic performance of the prepared catalyst of Pd nanoparticles immobilized on cage-like porous microspheres is tested by the catalytic hydrogenation of nitrobenzene at  $30\text{ }^\circ\text{C}$  in water, and an efficient and reusable heterogeneous Pd catalyst is demonstrated.

#### ■ ASSOCIATED CONTENT

**S Supporting Information.** Text as well as Figures S1–S8 showing the TEM image of the solid PS microspheres, the FTIR spectrum of the PS-*co*-PVBAH cage-like porous microspheres, the magnified TEM image of the solid PS-*co*-PVBAH microspheres synthesized with the weight ratio of VBA/St = 5/100, the TEM image of Pd immobilized on solid PS microspheres, the XPS spectrum of the 10-Pd@PS-*co*-PVBAH catalyst, the histogram of size distribution of the Pd nanoparticles in the catalysts, and the details on catalyst recycling. This material is available free of charge via the Internet at <http://pubs.acs.org>.

#### ■ AUTHOR INFORMATION

##### Corresponding Author

\*E-mail: wqzhang@nankai.edu.cn. Tel: 86-22-23509794. Fax: 86-22-23503510.

#### ■ ACKNOWLEDGMENT

The financial support by National Science Foundation of China (Nos. 20974051 and 21074059) and Tianjin Natural Science Foundation (No. 09JCYBJC02800) is gratefully acknowledged.

## REFERENCES

- (1) Letsinger, R. L.; Mahadevan, V. *J. Am. Chem. Soc.* **1966**, *88*, 5319–5324.
- (2) Uozumi, Y.; Nakao, R. *Angew. Chem., Int. Ed.* **2003**, *42*, 194–197.
- (3) Cho, J. K.; Najman, R.; Dean, T. W.; Ichihara, O.; Muller, C.; Bradley, M. *J. Am. Chem. Soc.* **2006**, *128*, 6276–6277.
- (4) Akiyama, R.; Kobayashi, S. *J. Am. Chem. Soc.* **2003**, *125*, 3412–3413.
- (5) Centomo, P.; Canton, P.; Ferronic, M.; Zecca, M. *New J. Chem.* **2010**, *34*, 2956–2961.
- (6) Ogasawara, S.; Kato, S. *J. Am. Chem. Soc.* **2010**, *132*, 4608–4613.
- (7) Hasell, T.; Wood, C. D.; Clowes, R.; Jones, J. T. A.; Khimiyak, Y. Z.; Adams, D. J.; Cooper, A. I. *Chem. Mater.* **2010**, *22*, 557–564.
- (8) He, J.; Kunitake, T.; Nakao, A. *Chem. Mater.* **2003**, *15*, 4401–4406.
- (9) El-Shall, M. S.; Abdelsayed, V.; Khder, A. E. R. S.; Hassan, H. M. A.; El-Kaderi, H. M.; Reich, T. E. *J. Mater. Chem.* **2009**, *19*, 7625–7631.
- (10) Lu, Y.; Mei, Y.; Schrunner, M.; Ballauff, M.; Möllner, M. W.; Breu, J. *J. Phys. Chem. C* **2007**, *111*, 7676–7681.
- (11) Mohammed, H. S.; Shipp, D. A. *Macromol. Rapid Commun.* **2006**, *27*, 1774–1778.
- (12) Michrowska, A.; Mennecke, K.; Kunz, U.; Kirschning, A.; Grela, K. *J. Am. Chem. Soc.* **2006**, *128*, 13261–13267.
- (13) Wen, F.; Zhang, W.; Wei, G.; Wang, Y.; Zhang, J.; Zhang, M.; Shi, L. *Chem. Mater.* **2008**, *20*, 2144–2150.
- (14) Zhang, J.; Xu, S.; Kumacheva, E. *J. Am. Chem. Soc.* **2004**, *126*, 7908–7914.
- (15) Hu, B.; Wu, T.; Ding, K.; Zhou, X.; Jiang, T.; Han, B. *J. Phys. Chem. C* **2010**, *114*, 3396–3400.
- (16) Okamoto, K.; Akiyama, R.; Yoshida, H.; Yoshida, T.; Kobayashi, S. *J. Am. Chem. Soc.* **2005**, *127*, 2125–2135.
- (17) Jaramillo, T. F.; Baeck, S.-H.; Cuenya, B. R.; McFarland, E. W. *J. Am. Chem. Soc.* **2003**, *125*, 7148–7149.
- (18) Cuenya, B. R.; Baeck, S.-H.; Jaramillo, T. F.; McFarland, E. W. *J. Am. Chem. Soc.* **2003**, *125*, 12928–12934.
- (19) Garcia-Martinez, J. C.; Lezutekong, R.; Crooks, R. M. *J. Am. Chem. Soc.* **2005**, *127*, 5097–5103.
- (20) Diallo, A. K.; Ornelas, C.; Salmon, L.; Aranzaes, J. R.; Astruc, D. *Angew. Chem., Int. Ed.* **2007**, *46*, 8644–8648.
- (21) Scott, R. W. J.; Wilson, O. M.; Oh, S.-K.; Kenik, E. A.; Crooks, R. M. *J. Am. Chem. Soc.* **2004**, *126*, 15583–15591.
- (22) Evangelisti, C.; Panziera, N.; D'Alessio, A.; Bertinetti, L.; Botavina, M.; Vitulli, G. *J. Catal.* **2010**, *272*, 246–252.
- (23) Tsunoyama, H.; Sakurai, H.; Negishi, Y.; Tsukuda, T. *J. Am. Chem. Soc.* **2005**, *127*, 9374–9375.
- (24) Seki, M. *Synthesis* **2006**, 2975–2992.
- (25) Phan, N. T. S.; Van Der Sluys, M.; Jones, C. W. *Adv. Synth. Catal.* **2006**, *348*, 609–679.
- (26) Thomas, J. M.; Johnson, B. F. G.; Raja, R.; Sankar, G.; Midgley, P. A. *Acc. Chem. Res.* **2003**, *36*, 20–30.
- (27) Benaglia, M.; Puglisi, A.; Cozzi, F. *Chem. Rev.* **2003**, *103*, 3401–3429.
- (28) Bergbreiter, D. E.; Sunga, S. D. *Adv. Synth. Catal.* **2006**, *348*, 1352–1366.
- (29) Djoos, B. M. L.; Vankelecom, I. F. J.; Jacobs, P. A. *Adv. Synth. Catal.* **2006**, *348*, 1413–1446.
- (30) Han, J.; Liu, Y.; Guo, R. *Adv. Funct. Mater.* **2009**, *19*, 1112–1117.
- (31) Gao, Y.; Ding, X.; Zheng, Z.; Cheng, X.; Peng, Y. *Chem. Commun.* **2007**, *36*, 3720–3722.
- (32) Miao, S.; Zhang, C.; Liu, Z.; Han, B.; Xie, Y.; Ding, S.; Yang, Z. *J. Phys. Chem. C* **2008**, *112*, 774–780.
- (33) Kim, J.-W.; Lee, J.-E.; Ryu, J.-H.; Lee, J.-S.; Kim, S.-J.; Han, S.-H.; Chang, I.-S.; Kang, H.-H.; Suh, K.-D. *J. Polym. Sci., Part A: Polym. Chem.* **2004**, *42*, 2551–2557.
- (34) Yang, L.; Zhang, M.; Lan, Y.; Zhang, W. *New J. Chem.* **2010**, *34*, 1355–1364.
- (35) Lan, Y.; Zhang, M.; Zhang, W.; Yang, L. *Chem.—Eur. J.* **2009**, *15*, 3670–3673.
- (36) Lan, Y.; Yang, L.; Zhang, M.; Zhang, W.; Wang, S. *ACS Appl. Mater. Interfaces* **2010**, *2*, 127–133.
- (37) He, X.; Ge, X.; Liu, H.; Wang, M.; Zhang, Z. *Chem. Mater.* **2005**, *17*, 5891–5892.
- (38) Caruso, F.; Caruso, R. A.; Möhwald, H. *Chem. Mater.* **1999**, *11*, 3309–3314.
- (39) Shi, X.; Briseno, A. L.; Sanedrin, R. J.; Zhou, F. *Macromolecules* **2003**, *36*, 4093–4098.
- (40) Lv, H.; Lin, Q.; Zhang, K.; Yu, K.; Yao, T.; Zhang, X.; Zhang, J.; Yang, B. *Langmuir* **2008**, *24*, 13736–13741.
- (41) Li, G.; Yang, X.; Wang, B.; Wang, J.; Yang, X. *Polymer* **2008**, *49*, 3436–3443.
- (42) Kobayashi, H.; Miyayama, E.; Okubo, M. *Langmuir* **2007**, *23*, 8703–8708.
- (43) Im, S. H.; Jeong, U.; Xia, Y. *Nature Mater.* **2005**, *4*, 671–675.
- (44) Li, G.; Xu, L.; Tang, X.; Neoh, K. G.; Kang, E. T. *Macromolecules* **2010**, *43*, 5797–5803.
- (45) Huang, C.-J.; Chang, F.-C. *Macromolecules* **2009**, *42*, 5155–5166.
- (46) Ali, M. M.; Stöver, H. D. H. *Macromolecules* **2003**, *36*, 1793–1801.
- (47) Zhang, H.; Cooper, A. I. *Chem. Mater.* **2002**, *14*, 4017–4020.
- (48) Sun, Q. H.; Deng, Y. L. *J. Am. Chem. Soc.* **2005**, *127*, 8274–8275.
- (49) Gao, F.; Su, Z.-G.; Wang, P.; Ma, G.-H. *Langmuir* **2009**, *25*, 3832–3838.
- (50) Gao, Q.; Wang, C.; Liu, H.; Chen, Y.; Tong, Z. *Polym. Chem.* **2010**, *1*, 75–77.
- (51) Hanson, J. A.; Chang, C. B.; Graves, S. M.; Li, Z.; Mason, T. G.; Deming, T. J. *Nature* **2008**, *455*, 85–89.
- (52) Wang, H.; Wang, M.; Ge, X. *Polymer* **2008**, *49*, 4974–4980.
- (53) Cao, Z.; Ziener, U.; Landfester, K. *Macromolecules* **2010**, *43*, 6353–6360.
- (54) Scott, C.; Wu, D.; Ho, C.-C.; Co, C. C. *J. Am. Chem. Soc.* **2005**, *127*, 4160–4161.
- (55) Kruk, M.; Jaroniec, M. *Chem. Mater.* **2001**, *13*, 3169–3183.
- (56) Wen, F.; Zhang, W.; Zheng, P.; Zhang, X.; Yang, X.; Wang, Y.; Jiang, X.; Wei, G.; Shi, L. *J. Polym. Sci., Part A: Polym. Chem.* **2008**, *46*, 1192–1202.
- (57) Zheng, P.; Zhang, W. *J. Catal.* **2007**, *250*, 324–330.
- (58) Klug, H. P.; Alexander, L. E. *X-ray Diffraction Procedures*; Wiley: New York, 1959.
- (59) Sangeetha, P.; Shanthi, K.; Rao, K. S. R.; Viswanathan, B.; Selvam, P. *Appl. Catal. A: General* **2009**, *353*, 160–165.
- (60) Liu, C.; Tan, R.; Yu, N.; Yin, D. *Microporous Mesoporous Mater.* **2010**, *131*, 162–169.
- (61) Raja, R.; Golovko, V. B.; Thomas, J. M.; Berenguer-Murcia, A.; Zhou, W.; Xie, S.; Johnson, B. F. G. *Chem. Commun.* **2005**, *15*, 2026–2028.
- (62) Mizukoshi, Y.; Sato, K.; Konno, T. J.; Masahashi, N.; Tanabe, S. *Chem. Lett.* **2008**, *37*, 922–923.
- (63) Islam, M.; Mondal, P.; Roy, A. S.; Tuhina, K. *Transition Met. Chem. (N. Y.)* **2010**, *35*, 427–435.
- (64) Samanta, S.; Nandi, A. K. *J. Phys. Chem. C* **2009**, *113*, 4721–4725.
- (65) Trapp, O.; Weber, S. K.; Bauch, S.; Bäcker, T.; Hofstadt, W.; Spliethoff, B. *Chem.—Eur. J.* **2008**, *14*, 4657–4666.